Title

Spectral evidence for unidirectional charge density wave in detwinned BaNi2As2

Permalink

https://escholarship.org/uc/item/7c59c6xn

Journal

Physical Review B, 108(8)

ISSN

2469-9950

Authors

Guo, Yucheng
Klemm, Mason
Oh, Ji Seop
et al.

Publication Date

2023-08-01

DOI

10.1103/physrevb.108.l081104

Peer reviewed

Spectral Evidence for Unidirectional Charge Density Wave in Detwinned BaNi$_2$As$_2$

Yucheng Guo,[1] Mason Klemm,[1] Ji Seop Oh,[1, 2] Yaofeng Xie,[1] Bing-Hua Lei,[3] Sergey Gorovikov,[4] Tor Pedersen,[4] Matteo Michiardi,[5, 6, 7] Sergey Zhdanovich,[5, 6] Andrea Damascelli,[5, 6] Jonathan Denlinger,[8] Makoto Hashimoto,[9] Donghui Lu,[9] Sung-Kwan Mo,[8] Rob G. Moore,[10] Robert J. Birgeneau,[2] David J. Singh,[3, 11] Pengcheng Dai,[1] and Ming Yi[1, *]

[1]*Department of Physics and Astronomy, Rice University, Houston, 77005 Texas, USA*
[2]*Department of Physics, University of California, Berkeley, 94720 California, USA*
[3]*Department of Physics and Astronomy, University of Missouri, Columbia, 65211 Missouri , USA*
[4]*Canadian Light Source Inc., University of Saskatchewan, Saskatoon, SK S7N 2V3, Canada*
[5]*Department of Physics and Astronomy, University of British Columbia, Vancouver, BC V6T 1Z1, Canada*
[6]*Quantum Matter Institute, University of British Columbia, Vancouver BC V6T 1Z4, Canada*
[7]*Max Planck Institute for Chemical Physics of Solids, Nöthnitzer Straße 40, 01187 Dresden, Germany*
[8]*Lawrence Berkeley National Laboratory, Berkeley, 94720 California, USA*
[9]*Stanford Synchrotron Radiation Lightsource, SLAC National Acelerator Laboratory, Menlo Park, 94025 California, USA*
[10]*Materials Science and Technology Division,Oak Ridge National Laboratory, Oak Ridge, 37831 Tennessee, USA*
[11]*Department of Chemistry, University of Missouri, Columbia, 65211 Missouri, USA*
(Dated: May 31, 2022)

The emergence of unconventional superconductivity in proximity to intertwined electronic orders is especially relevant in the case of iron-based superconductors. Such order consists of an electronic nematic order and a spin density wave in these systems. BaNi$_2$As$_2$, like its well-known iron-based analog BaFe$_2$As$_2$, also hosts a symmetry-breaking structural transition that is coupled to a unidirectional charge density wave (CDW), providing a novel platform to study intertwined orders. Here, through a systematic angle-resolved photoemission spectroscopy study combined with a detwinning B_{1g} uniaxial strain, we identify distinct spectral evidence of band evolution due to the structural transition as well as CDW-induced band folding. In contrast to the nematicity and spin density wave in BaFe$_2$As$_2$, the structural and CDW order parameters in BaNi$_2$As$_2$ are observed to be strongly coupled and do not separate in the presence of uniaxial strain. Our measurements point to a likely lattice origin of the CDW in BaNi$_2$As$_2$.

Quantum materials hosting unconventional superconductivity tend to develop complex phase diagrams where multiple electronic orders interact. In the Fe-based superconductors (FeSCs), the ubiquitous intertwined order takes form in a C$_4$-rotational symmetry-breaking nematic phase and a spin density wave (SDW) [1–3]. The nematic order manifests in a tetragonal to orthorhombic structural transition, identified as electronically driven by a divergent nematic susceptibility from elastoresistance measurements [4]. Additionally, rotational symmetry-breaking is observed in the electronic, magnetic and optical properties [5–12]. Superconductivity emerges when these competing orders are suppressed by either doping or pressure, resulting in T_c as high as 40 K [13, 14].

BaNi$_2$As$_2$–a nickel-based analog of the well-studied FeSC BaFe$_2$As$_2$–shares the same high temperature tetragonal phase [15]. Distinct from BaFe$_2$As$_2$, BaNi$_2$As$_2$ is nonmagnetic and superconducts with a T_c of 0.6K [16]. Instead of the coupled nematicity and SDW found in BaFe$_2$As$_2$, BaNi$_2$As$_2$ exhibits a symmetry-lowering structural transition into a triclinic phase at T_S =136 K accompanied by unconventional charge density waves (CDWs). The progression from the tetragonal state to the triclinic state is still under debate. From x-ray diffraction, Lee. *et al.* discovered that the CDW first appears in the tetragonal state as an incommensurate order (IC-CDW), then transits to a different uni-

directional IC-CDW at T_S and then locks into a commensurate order (C-CDW) below T_S [17, 18]. The crystal structure in this picture changes from tetragonal directly to triclinic at T_S in a first order transition. Recent dilatometry work suggests that the crystal structure explicitly breaks C$_4$ rotational symmetry in the form of a orthorhombic phase in a second order transition before additional symmetry-lowering into the triclinic phase at T_S in a first-order fashion [19]. Substitution of either Co on the Ni site or Sr on the Ba site can completely suppress the triclinic phase and the associated CDW orders, reaching a maximum T_c of 3.5 K. Elastoresistance measurements show that Ba$_{1-x}$Sr$_x$Ni$_2$As$_2$ exhibits a diverging nematic susceptibility in the B_{1g} channel, which may be the cause for the enhancement of T_c near optimal doping [20]. A Ginzburg–Landau analysis suggests that the divergence of nematic susceptibility in Ba$_{1-x}$Sr$_x$Ni$_2$As$_2$ could be driven by either lattice or electronic degrees of freedom, in contrast to BaFe$_2$As$_2$, where the divergence in the B_{2g} channel is electronically-driven. BaNi$_2$As$_2$ therefore offers a rich platform to investigate intertwined orders, where the electronic structure could provide important insights into the nature of nematicity, CDWs, and their connection to unconventional superconductivity. Here, using angle-resolved photoemission spectroscopy (ARPES) under uniaxial strain, we probe the electronic structure evolution of BaNi$_2$As$_2$
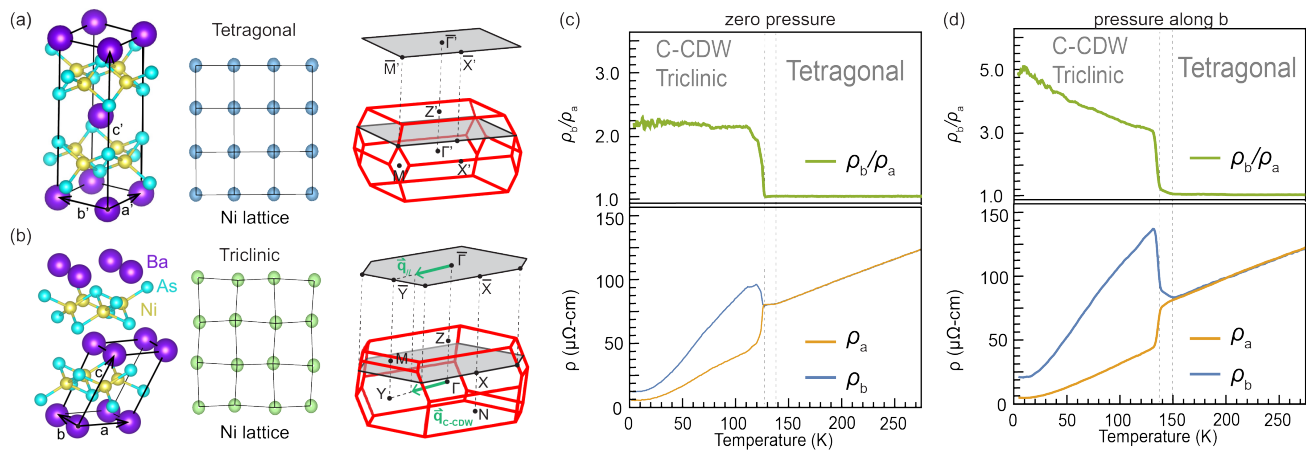
FIG. 1. (a)-(b) Crystal structure and BZ for the tetragonal and triclinic phases. The red (gray) BZ represents the 3D (2D projected) BZ. The green arrows in (b) denote the q-vectors for C-CDW and its in-plane component. (c)-(d) Temperature-dependent in-plane resistivity ρ_a (yellow), ρ_b(blue) and ρ_b/ρ_a(green) with and without uniaxial compressive strain along b.

across the phase transitions. We find no evidence of Fermi surface nesting in the tetragonal state, unidirectional band folding consistent with the reported C-CDW q-vector in the C-CDW/triclinic state, and rotational symmetry-breaking that onsets abruptly at the triclinic transition. Furthermore, the extracted temperature evolution of the spectral features identifies a distinct order parameter for the C-CDW from the triclinic structural transition. However, the two order parameters are observed to be strongly coupled even in the presence of uniaxial strain, distinct from the case of $BaFe_2As_2$ where strain lifts the nematic band splitting to onset well above that of the SDW phase. Our results taken together suggest a strongly lattice-driven intertwined order in parent $BaNi_2As_2$ and much weaker nematic fluctuations compared to that of the FeSC $BaFe_2As_2$.

High-quality single crystals of $BaNi_2As_2$ were synthesized using the self-flux method [15]. Resistivity measurements were carried out in a Quantum Design Physical Properties Measurement System using a clamp to supply an in-plane, uniaxial pressure. [21] ARPES measurements were performed at the QMSC beamline at the Canadian Light Source, beamlines 4.0.3 and 10.0.1 of the Advanced Light Source, and beamline 5-2 of the Stanford Synchrotron Radiation Lightsource with electron analyzers at an energy and angular resolution of 12 meV and 0.1°, respectively. The samples were cleaved *in-situ* with base pressures below 5×10^{-11} Torr. The polarization used was circular left (CL) unless otherwise noted. To avoid the domain mixing effect, we used a mechanical clamp to detwin the $BaNi_2As_2$ crystals along the [010] direction, with a typical pressure of 5-10 MPa [22].

At room temperature, tetragonal $BaNi_2As_2$ belongs to the space group I4/mmm (a=4.142Å, c=11.65Å) (Fig. 1(a)). It undergoes a first-order phase transition

to the triclinic structure (a=4.21Å, b=3.99Å, c=6.31Å, α=105.2°, β=108.6°, γ=89.3°, space group P$\bar{1}$) at T_S = 136K (Fig. 1(b)). The corresponding 3D Brillouin Zones (BZ) of the tetragonal and triclinic phases are shown accordingly, where the rotational C_4 symmetry is broken for the triclinic phase. The C-CDW q-vector in the triclinic state is denoted by q_{C-CDW}, which does not lie in the projected BZ plane while its in-plane component ($q_{//}$) is very close to one third of the projected tetragonal BZ (See SM). We carried out temperature dependent in-plane electrical resistivity measurements along with two orthogonal directions with and without uniaxial pressure. In contrast to $BaFe_2As_2$ [21], even in the absence of a detwinning stress, we observe resistivity anisotropy (ρ_b-ρ_a) below T_S, signaling a strong structural distortion and associated unequal domain populations. In the presence of stress, the resistivity anisotropy is enhanced, demonstrating that the applied uniaxial stress redistributes the domain populations. In addition, we observe a kink above T_S in the zero-stress sample, which is likely the reported IC-CDW transition [17]. In the measurement under stress, the kink feature is replaced by the onset of the resistivity anisotropy, which can be interpreted as either a detwinning effect of the crystal orthorhombic domains [5], or strain-induced rotational symmetry-breaking [23]. It is interesting to point out that, in contrast to $BaFe_2As_2$, the uniaxial pressure does not broaden the structural transition [21, 24].

To visualize the electronic structure of $BaNi_2As_2$, we present ARPES measurements taken in the tetragonal phase. The Fermi surface maps (FSMs) and band dispersions along high symmetry directions correspond to the k_z=0 (Fig. 2(a)-(b)) and k_z =$\pi/2$ (Fig. 2(c)-(d)) planes are taken with 60 eV and 79 eV photons, respectively (Fig. 2(e)). The C_4 symmetry of the tetragonal state
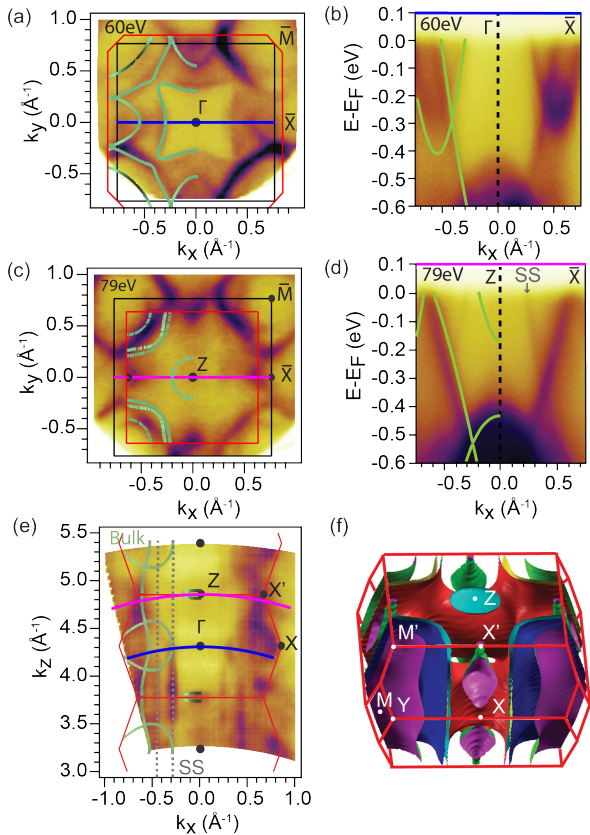
FIG. 2. Electronic structure in the tetragonal state (170 K). (a) Fermi surface (FS) measured with 60 eV photons ($k_z =0$). (b) Band dispersions measured along Γ-X as marked in (a). (c)-(d) Same as (a)-(b) but measured with 79 eV photons ($k_z =\pi$). (e) Photon energy-dependent measurement in the k_x-k_z plane, with an inner potential of 15 eV. (f) DFT calculation of the 3D FSs. In addition, DFT calculated band dispersions and FSs are overlaid on all data in green solid lines. Grey arrow and dashed lines mark the surface states. All data taken with circular right (CR) polarization.

is observed, and there is overall good agreement with Density Functional Theory (DFT) calculations, consistent with previous ARPES reports on $BaNi_2As_2$ [25, 26]. The electronic structure exhibits strong k_z dispersion. The most intense Fermi surfaces are large pockets around the M points. Besides dispersive bulk states, there exists surface states which are not dispersive along k_z and have no correspondence in the bulk band calculations (denoted by SS, see SM for more details).

Having identified the electronic structure in the tetragonal state, we now examine the low temperature triclinic phase. To probe the intrinsic single-domain electronic structure, we apply uniaxial compressive strain along the crystal axis [010], which aligns all the domains along the shorter b-axis. The main features of the low temperature FSM of the strained crystal (Fig. 3(a)) resemble their tetragonal counterparts except for the appearance of new bands marked in cyan, which can be understood as

folded copies of the M pocket that only appear along the b-direction, hence breaking the rotational C_4 symmetry. This anisotropy can be demonstrated by a comparison of the momentum distribution curve (MDC) taken at equivalent momenta along the k_x and k_y directions, where only a peak is seen across the folded feature (Fig. 3(e)). Such band folding is a signature of translational symmetry breaking. We note that the folding vector is approximately $\frac{1}{3}$, which is consistent with the in-plane projection of the q_{C-CDW} observed by x-ray diffraction [17, 26]. Therefore, this band folding is a signature of the unidirectional CDW, which was not observed in previous ARPES studies of $BaNi_2As_2$ [25].

To exclude rotational symmetry-breaking effect due to extrinsic photoemission matrix elements, we measured the strained sample in a geometry where the a and b directions are symmetric with respect to the analyzer slit (Fig. 3). In this geometry, the photoemission matrix elements are equivalent along the k_x and k_y directions therefore any observed difference must be intrinsic to the band structure. We note that the folded bands still only appear along the strained direction, reflecting a true C_2 symmetry. In addition, above the CDW ordering temperature (Fig. 3(b)), the folded bands in the strained sample disappear, restoring the C_4 symmetry, as also confirmed by the disappearance of the peak in the MDC (Fig. 1(e)). For comparison, the FSM of an unstrained twinned crystal (Fig. 3(d)) shows folded bands in both directions, consistent with the understanding of unidirectional CDW folding under mixed domains. The comparison between the FSMs of the strained and unstrained crystals clearly establishes that uniaxial strain is effective at detwinning the crystal and important for resolving the observed CDW band folding. We also note that besides the bulk bands described here, we observed a set of surface states (SS) that strongly reflects a broken C_4 symmetry observed in strained crystals, demonstrating the effectiveness of the applied strain (See SM). These states have no correspondence in the bulk DFT calculated bands and do not disperse with k_z, consistent with a surface origin.

Next, we examine in detail the evolution of the rotational and translational symmetry breaking in the electronic structure. Specifically, we traced the dispersions along the the $\bar{\Gamma}$-$\bar{X}$ and $\bar{\Gamma}$-$\bar{Y}$ directions measured on detwinned crystals as a function of temperature (Fig. 4). While dispersions along the two orthogonal directions are identical in the tetragonal phase (170 K), bands are strongly modified in the low temperature phase (100 K), with band crossing only along $\bar{\Gamma}$-$\bar{X}$ but not along $\bar{\Gamma}$-$\bar{Y}$ (Fig. 4(b)-(g)). To understand the observed dispersions, we illustrate with a schematic in Fig. 4(a). In the normal state above T_{IC-CDW}, the Fermi surface consists of large pockets around the $\bar{M}$ points. Two types of transitions occur that modify the bands. First, the structural transition from tetragonal to triclinic is reflected in a bro-
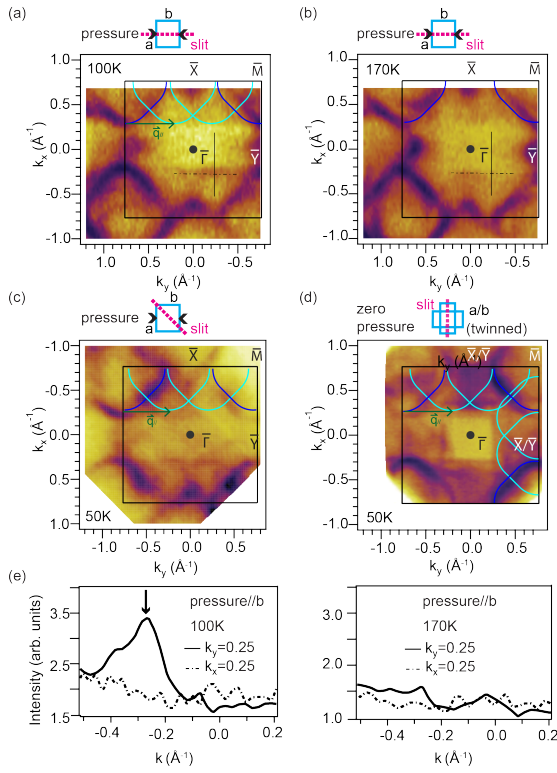
FIG. 3. FSs of detwinned BaNi$_2$As$_2$. (a) FS taken at 79 eV in the triclinic phase (100K) with horizontal compressive uniaxial pressure. (b) Same as (a) but taken in the tetragonal phase (170K). (c) Same as (a) but taken at 50K with a 45° analyzer slit direction. (d) FS taken with CR 60eV photons at 50K without uniaxial pressure. Blue lines mark the Fermi pockets around $\bar{M}$, while cyan lines indicate bands folded from the $\bar{M}$ points due to the C-CDW. (e) MDCs along k$_y$=0.25Å^{-1} (solid line) and k_x=0.25Å^{-1} (dashed line) for strained sample at 100K and 170K respectively, as marked in (a)-(b). The black arrow denotes the folded feature.

ken rotational symmetry, where the blue dispersion bends down along $\bar{\Gamma}$-$\bar{Y}$. Second, the unidirectional CDW folds the M pockets along k_y, resulting in a folded parabolic band (cyan) that only appears along $\bar{\Gamma}$-$\bar{X}$.

We then use the spectral signatures of these two types of symmetry breaking to trace out their order parameters. First, we trace the spectral signature associated with the rotational symmetry breaking in the form of the band shift along $\bar{\Gamma}$-$\bar{Y}$. As captured by MDC3 in Fig. 4(e),(h), an abrupt change occurs at T_S in a strongly first-order fashion. This is also reflected in the apparent jump in the temperature-dependent spectral weight integrated across the gray momentum range (Fig. 4(h)-(i)). Second, we trace the band folding by comparing the MDC across the cyan band for $\bar{\Gamma}$-$\bar{X}$ and $\bar{\Gamma}$-$\bar{Y}$ (Fig. 4(h)). The presence of the folded band is seen in a hump in the MDC along $\bar{\Gamma}$-$\bar{X}$ (MDC1) but not $\bar{\Gamma}$-$\bar{Y}$ (MDC2). The spectral weight of the hump gradually decreases as the temperature is raised, confirmed by the integrated spectral weight

in the marked momentum range plotted against temperature, which mimics the behavior of a second order phase transition (Fig. 4(j)). This is in contrast to the abrupt jump of the rotational symmetry-breaking in Fig. 4(i), suggesting that the CDW and triclinic structural transition have distinct order parameters.

Comparing the two extracted order parameters, we note that both appear to onset simultaneously in a single phase transition within our experimental uncertainty, although the CDW band folding order parameter evolves much more smoothly than that of the band shift. This contrast is also apparent in the collapsed MDC curves in Fig. 4(h). Due to the abrupt onset, we ascribe the band shift transition to the first-order structural transition into the triclinic phase. While a small kink is observed above T_S in the resistivity indicating the onset of IC-CDW and potential orthorhombic transition and nematic order, we do not observe any apparent change in the band dispersions above T_S (see SM). This does not preclude the existence of a nematic phase above T_S, but rather indicates that the energy scale of the symmetry-breaking in the electronic structure associated with IC-CDW and nematic order is much smaller than that observed for the nematic phase in BaFe$_2$As$_2$.

Finally, we study the effect of uniaxial strain on the order parameters extracted from the spectral signatures. The spectral weights acquired from unstrained crystals by following the same procedures described above are plotted in (Fig. 4(i)-(j)), showing very similar behavior as those obtained on strained samples. In particular, we observe no elevation in the onset temperature of either order parameter in the warming up measurement. This is again in contrast to BaFe$_2$As$_2$ (Fig. 4(k)), where the uniaxial strain clearly elevates the onset temperature of the observed orbital anisotropy and separates it from the SDW ordering temperature [27]. The results taken together suggest that the translational symmetry-breaking of the C-CDW and the structural transition into the triclinic phase are strongly coupled in BaNi$_2$As$_2$, and that nematic fluctuations are much weaker than that in BaFe$_2$As$_2$. The C-CDW, from a lack of Fermi surface nesting conditions, is likely dominated by lattice. The recent DFT results show that two distinct structures compete due to complex As bonding patterns and drive distortions of the Ni layers which possibly explain the unconventional CDW behavior of the ground state [28].

In the broader context of FeSCs, the coupling of the nematic and magnetic order varies as well. In BaFe$_2$As$_2$, the structural transition is second-order, followed by a first-order magnetic transition. In the structural homolog SrFe$_2$As$_2$, the structural and magnetic transitions are strongly first-order and occur simultaneously. Uniaxial strain also does little in harvesting the nematic fluctuations above T_S [24]. The case of BaNi$_2$As$_2$ as we demonstrate here, appears to be similar in spirit to that of SrFe$_2$As$_2$, where very weak rotational symmetry-
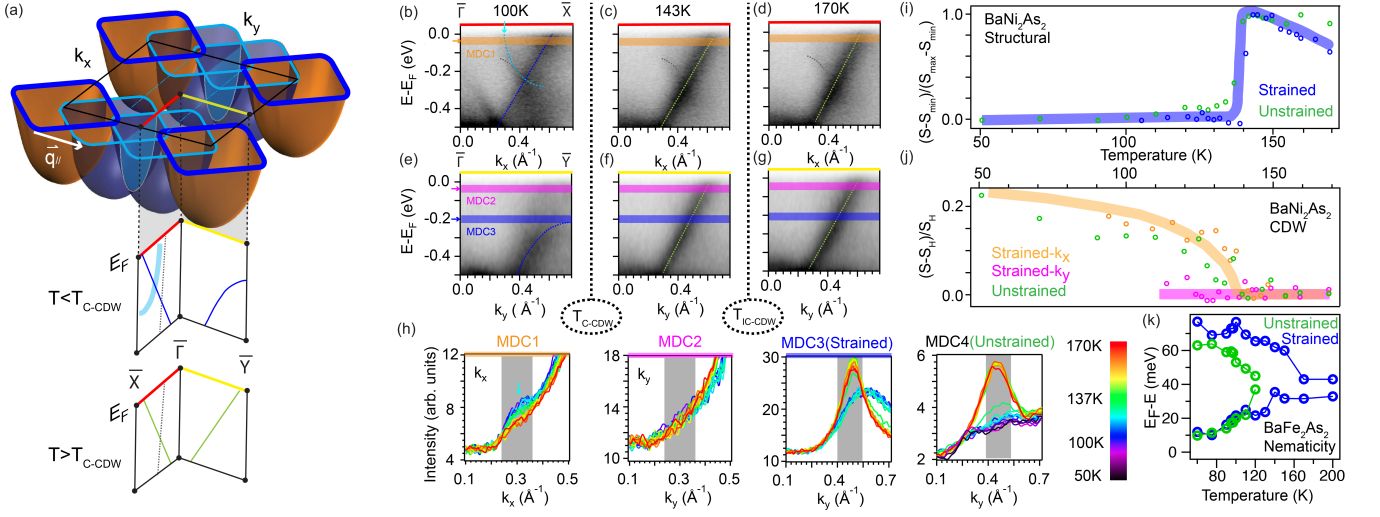
FIG. 4. Temperature evolution through the CDW transitions on detwinned $BaNi_2As_2$. (a) Summary of the band evolution across T_{C-CDW}. (b)-(d) Temperature dependence of band dispersions along $\bar{\Gamma}$-$\bar{X}$ for (b) T < T_{C-CDW}, (c) T_{C-CDW} < T < T_{IC-CDW}, and (d) T > T_{IC-CDW}. (e)-(g) Same as (b)-(d) but taken along $\bar{\Gamma}$-$\bar{Y}$. Dashed line are guides to the eyes. (h) Temperature dependence of MDCs as marked in (b)-(g). The locations of MDCs are as marked. (i) Integrated spectral weight as a function of temperature within the gray window for MDC3 and MDC4. Each curve is normalized to the maximum spectral weight. (j) Integrated spectral weight within the gray window in MDC1 and MDC2 and the equivalent MDC taken on the unstained crystal as a function of temperature. Each curve is normalized by calculating $(S-S_H)/S_H$, where S_H is the average spectral weight between 145K-170K. Solid lines are guides to the eyes. (k) Temperature evolution of d_{xz} and d_{yz} band positions in $BaFe_2As_2$ with and without uniaxial strain (reproduced from [5]).

breaking exists above the strongly first-order structural transition. However, with substitution of P on the As site or Sr on the Ba site, nematic fluctuations appear to grow both in the size of the anisotropic thermal expansion above T_S [19], as well as a diverging nematic susceptibility, which have been proposed to be responsible for the enhancement of T_c [20]. $BaNi_2As_2$ therefore offers a rich platform analogous to the magnetic FeSCs where intertwined order from the charge-nematic sector interacts with superconductivity.

* mingyi@rice.edu

[1] F. Wang, S. A. Kivelson, and D.-H. Lee, Nat. Phys. **11**, 959 (2015).

[2] Q. Wang, Y. Shen, B. Pan, Y. Hao, M. Ma, F. Zhou, P. Steffens, K. Schmalzl, T. R. Forrest, M. Abdel-Hafiez,

X. Chen, D. A. Chareev, A. N. Vasiliev, P. Bourges, Y. Sidis, H. Cao, and J. Zhao, Nat. Mater. **15**, 159 (2016).

[3] P. Dai, Rev. Mod. Phys. **87**, 855 (2015).

[4] J. H. Chu, H. H. Kuo, J. G. Analytis, and I. R. Fisher, Science **337**, 710 (2012).

[5] M. Yi, D. Lu, J.-H. Chu, J. G. Analytis, A. P. Sorini, A. F. Kemper, and B. Moritz, Proc. Natl. Acad. Sci. U.S.A. **108**, 6878 (2011).

[6] J. Zhao, D. T. Adroja, D.-X. Yao, R. Bewley, S. Li, X. F. Wang, G. Wu, X. H. Chen, J. Hu, and P. Dai, Nat. Phys. **5**, 555 (2009).

[7] T.-M. Chuang, M. P. Allan, J. Lee, Y. Xie, N. Ni, S. L. Bud'ko, G. S. Boebinger, P. C. Canfield, and J. C. Davis, Science **327**, 181 (2010).

[8] C. C. Homes, T. Wolf, and C. Meingast, Phys. Rev. B Condens. Matter **102**, 155135 (2020).

[9] C. Dhital, Z. Yamani, W. Tian, J. Zeretsky, A. S. Sefat, Z. Wang, R. J. Birgeneau, and S. D. Wilson, Phys. Rev. Lett. **108**, 087001 (2012).

[10] M. A. Tanatar, E. C. Blomberg, A. Kreyssig, M. G. Kim, N. Ni, A. N. Thaler, S. L. Bud'ko, P. C. Canfield, A. I. Goldman, I. I. Mazin, and R. Prozorov, Physical Review B (2010).

[11] S.-H. Baek, D. V. Efremov, J. M. Ok, J. S. Kim, J. van den Brink, and B. Büchner, Phys. Rev. B Condens. Matter **93**, 180502 (2016).

[12] J. L. Niedziela, D. Parshall, K. A. Lokshin, A. S. Sefat, A. Alatas, and T. Egami, Phys. Rev. B Condens. Matter **84**, 224305 (2011).

[13] H. Takahashi, K. Igawa, K. Arii, Y. Kamihara, M. Hirano, and H. Hosono, Nature **453**, 376 (2008).

[14] Y. Mizuguchi, Y. Hara, K. Deguchi, S. Tsuda, T. Yamaguchi, K. Takeda, H. Kotegawa, H. Tou, and Y. Takano, Supercond. Sci. Technol. **23**, 054013 (2010).

[15] A. S. Sefat, M. A. McGuire, R. Jin, B. C. Sales, D. Mandrus, F. Ronning, E. D. Bauer, and Y. Mozharivskyj, Phys. Rev. B Condens. Matter **79**, 094508 (2009).

[16] F. Ronning, N. Kurita, E. D. Bauer, B. L. Scott, T. Park, T. Klimczuk, R. Movshovich, and J. D. Thompson, Europhysics Letters **20**, 342203 (2008).

[17] S. Lee, G. De La Peña, S. X. L. Sun, M. Mitrano, Y. Fang, H. Jang, J. S. Lee, C. Eckberg, D. Campbell, J. Collini, J. Paglione, F. M. F. De Groot, and P. Abbamonte, Phys. Rev. Lett. **122**, 147601 (2019).

[18] S. Lee, J. Collini, S. X.-L. Sun, M. Mitrano, X. Guo, C. Eckberg, J. Paglione, E. Fradkin, and P. Abbamonte, Phys. Rev. Lett. **127**, 027602 (2021).

[19] M. Merz, L. Wang, T. Wolf, P. Nagel, C. Meingast, and S. Schuppler, Phys. Rev. B Condens. Matter **104**, 184509 (2021).

[20] C. Eckberg, D. J. Campbell, T. Metz, J. Collini, H. Hodovanets, T. Drye, P. Zavalij, M. H. Christensen, R. M. Fernandes, S. Lee, P. Abbamonte, J. W. Lynn, and J. Paglione, Nat. Phys. **16**, 346 (2020).

[21] J. H. Chu, J. G. Analytis, K. De Greve, P. L. McMahon, Z. Islam, Y. Yamamoto, and I. R. Fisher, Science **329**, 824 (2010).

[22] I. R. Fisher, L. Degiorgi, and Z. X. Shen, Rep. Prog. Phys. **74**, 124506 (2011).

[23] Y. Song, D. Yuan, X. Lu, Z. Xu, E. Bourret-Courchesne, and R. J. Birgeneau, Phys. Rev. Lett. **123**, 247205 (2019).

[24] D. W. Tam, W. Wang, L. Zhang, Y. Song, R. Zhang, S. V. Carr, H. C. Walker, T. G. Perring, D. T. Adroja, and P. Dai, Phys. Rev. B Condens. Matter **99** (2019).

[25] B. Zhou, M. Xu, Y. Zhang, G. Xu, C. He, L. X. Yang, F. Chen, B. P. Xie, X. Y. Cui, M. Arita, K. Shimada, H. Namatame, M. Taniguchi, X. Dai, and D. L. Feng, Phys. Rev. B **83**, 1 (2011).

[26] N. S. Pavlov, T. K. Kim, A. Yaresko, K.-Y. Choi, I. A. Nekrasov, and D. V. Evtushinsky, J. Phys. Chem. C **125**, 28075 (2021).

[27] Y. Song, S. V. Carr, X. Lu, C. Zhang, Z. C. Sims, N. F. Luttrell, S. Chi, Y. Zhao, J. W. Lynn, and P. Dai, Phys. Rev. B Condens. Matter **87**, 184511 (2013).

[28] B.-H. Lei, Y. Guo, Y. Xie, P. Dai, M. Yi, and D. J. Singh, Phys. Rev. B Condens. Matter **105**, 144505 (2022).